Supporting Information

A highly integrated blade structure for thermoelectric devices with ultra-high output voltage and power densities

Chuanyao Sun[1,2], Pengfei Qiu[1,2,3]*, Xinjie Yuan[1,2], Kelin Shen[1,2], Yi Wu[1,2], Xuefeng Zhao[1], Jiawei Zhang[1], Shiqi Yang[1], Lidong Chen[1,2], Xun Shi[1,2]*

[1]State Key Laboratory of High Performance Ceramics, Shanghai Institute of Ceramics, Chinese Academy of Sciences, Shanghai 200050, China

[2]Center of Materials Science and Optoelectronics Engineering, University of Chinese Academy of Sciences, Beijing 100049, China

[3]School of Chemistry and Materials Science, Hangzhou Institute for Advanced Study, University of Chinese Academy of Sciences, Hangzhou 310024, China

*Corresponding authors.

E-mails: qiupf@mail.sic.ac.cn; xshi@mail.sic.ac.cn.

Note 1: Voltage density and power density

Herein, a simplified one-dimensional steady-state heat transfer model is adopted to derive the voltage density (V_{oc}/A) and power density (P_{max}/A). In this model, the thermal resistance between the TE leg and the heat source is neglected. The cold end of the TE leg is directly exposed to air. The heat transfer obeys one-dimensional model. The schematics is shown in **Fig. S12**. The open-circuit voltage (V_{oc}) and maximum output power (P_{max}) of this TE leg can be simply expressed as

$$V_{oc} = n\alpha T_{eff} \tag{1}$$

$$P_{max} = \frac{V_{oc}^2}{4R_{in}} \tag{2}$$

where n is the number of TE legs, α is the Seebeck coefficient, and T_{eff} is the temperature difference on the TE leg.

The internal resistance (R_{in}) of this TE leg is described as

$$R_{in=} n \cdot \frac{H}{\sigma \cdot S_{leg}} \tag{3}$$

where H is the height of TE legs, S_{leg} is the cross-sectional area of a single TE leg, σ is the electrical conductivity of the TE material.

Substituting Equations (1) and (3) into Equation (2) yields

$$P_{max} = \frac{n \cdot \alpha^2 \cdot T_{eff}^2}{4 \cdot \frac{H}{\sigma \cdot S_{leg}}} \tag{4}$$

In this case, the thermal resistance of the TE legs (θ_{TE}), the thermal resistance between the air and TED (θ_{Air}), and the T_{eff} can be expressed as

$$\theta_{TE} = \frac{H}{\kappa \cdot n \cdot S_{leg}} \tag{5}$$

$$\theta_{Air} = \frac{1}{h_{air} \cdot A} \tag{6}$$

$$T_{eff} = T_{tol}\frac{\theta_{TE}}{\theta_{Air} + \theta_{TE}} = T_{tol}\frac{\frac{H}{\kappa \cdot n \cdot S_{leg}}}{\frac{1}{h_{air} \cdot A} + \frac{H}{\kappa \cdot n \cdot S_{leg}}} \tag{7}$$

where A is the total cross-sectional area of the TE device, H is the height of TE legs, T_{tol} is the temperature difference between the human body and the ambient environment, κ is the thermal conductivity of the TE material.

Then, the voltage density (V_{oc}/A) and power density (P_{max}/A) can be expressed as

$$\frac{V_{oc}}{A} = \alpha T_{tol} \cdot \frac{\frac{H}{S_{leg}} \cdot \frac{1}{\kappa}}{\frac{1}{h_{air}} + \frac{1}{\kappa} \cdot \frac{H}{S_{leg}} \cdot \frac{A}{n}} \tag{8}$$

$$\frac{P_{max}}{A} = \frac{PF \cdot T_{tol}^2}{4\kappa} \cdot \frac{\frac{1}{\kappa} \cdot \frac{H}{S_{leg}} \cdot \frac{A}{n}}{(\frac{1}{h_{air}} + \frac{1}{\kappa} \cdot \frac{H}{S_{leg}} \cdot \frac{A}{n})^2} \quad (9)$$

Where *PF* is the power factor of the TE material.

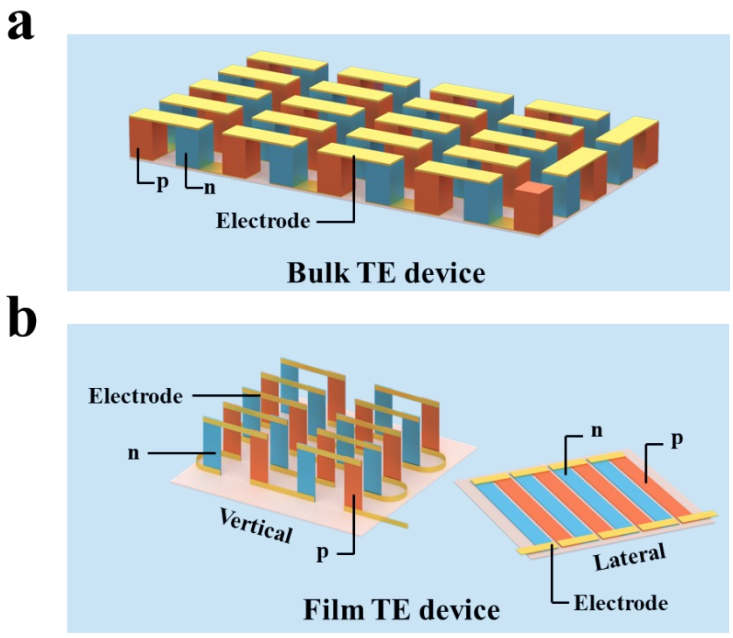

Fig. S1 Sketch maps of (a) a conventional bulk TE device and (b) typical film TE devices.

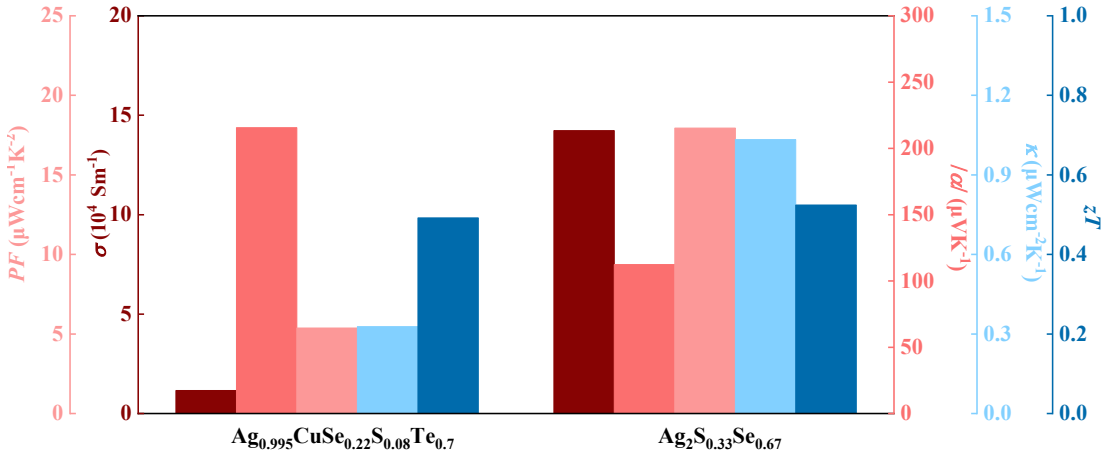

Fig. S2 TE properties of the $Ag_2S_{0.33}Se_{0.67}$ and $Ag_{0.995}CuSe_{0.22}S_{0.08}Te_{0.7}$ bulks at room temperature.

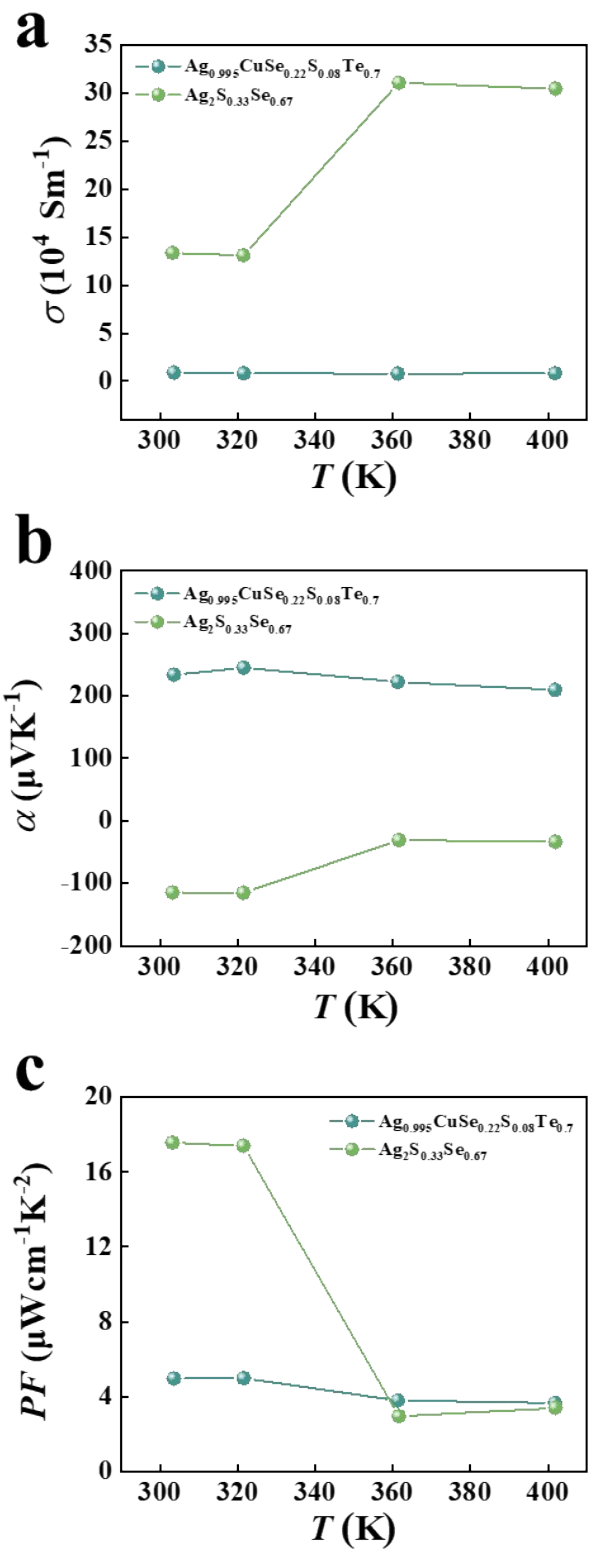

Fig. S3 TE properties of the $Ag_2S_{0.33}Se_{0.67}$ and $Ag_{0.995}CuSe_{0.22}S_{0.08}Te_{0.7}$ films with the thickness of 60 μm. (a) Temperature dependences of electrical conductivity (σ), (b) Seebeck coefficient (α), and (c) power factor (PF).

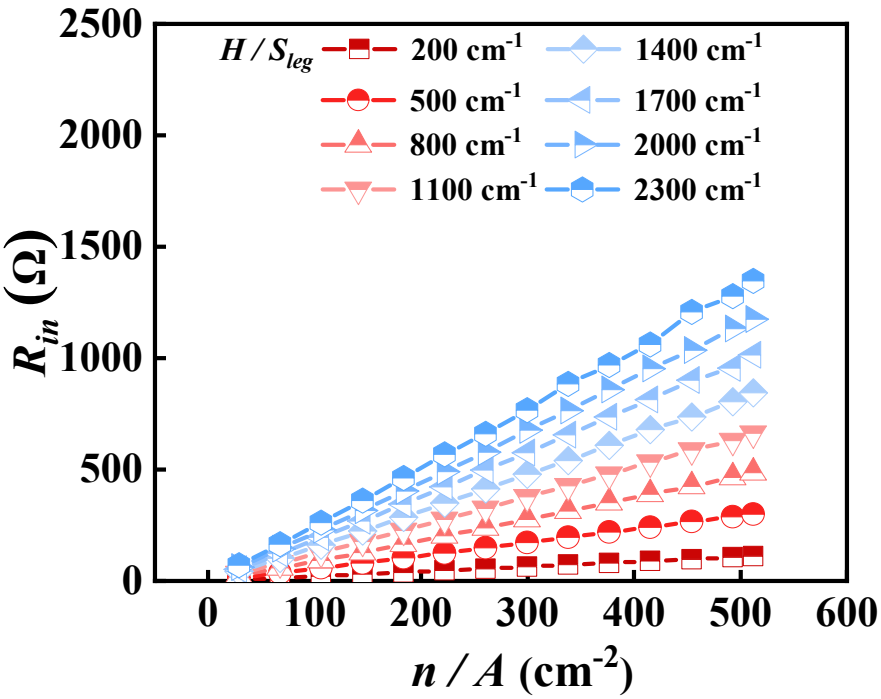

Fig. S4 Simulated internal resistance (R_{in}) as a function of n/A for the blade TE device with different H/S_{leg}.

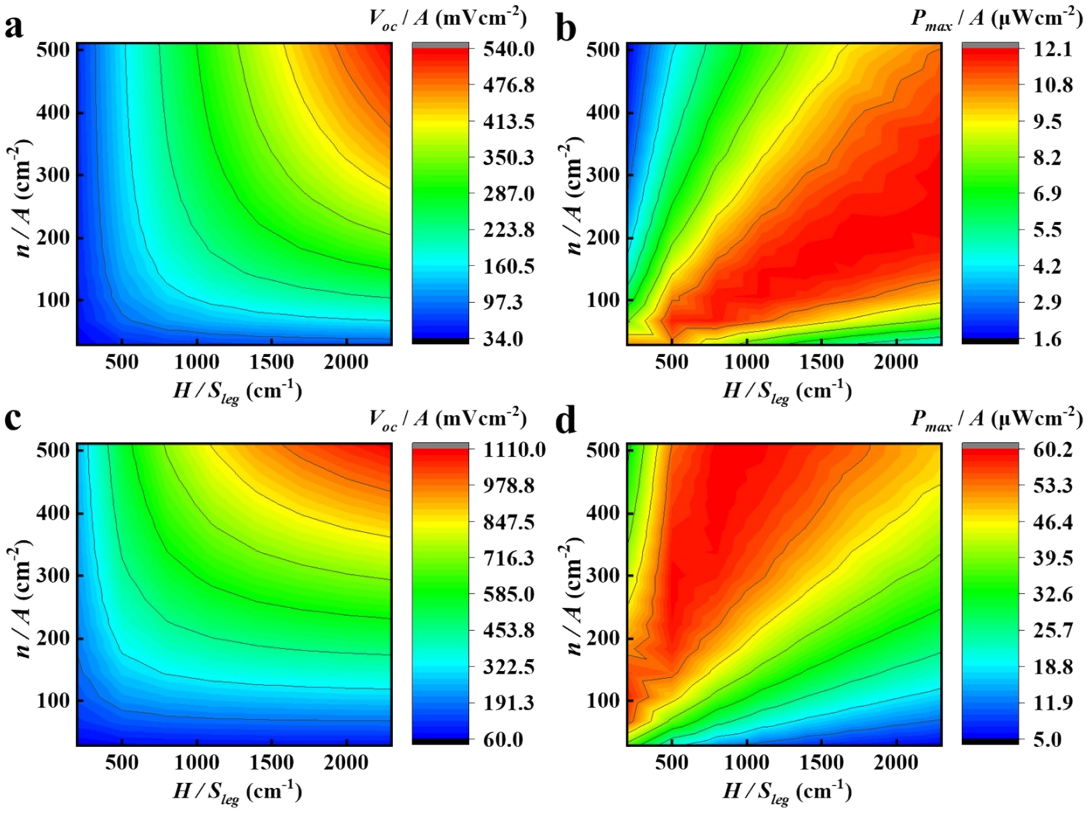

Fig. S5 Cloud charts illustrating the relationships among n/A, H/S_{leg}, V_{oc}/A, and P_{max}/A at convective heat transfer coefficient of (a, b) 10 Wm^{-2}K^{-1} and (c, d) 50 Wm^{-2}K^{-1}.

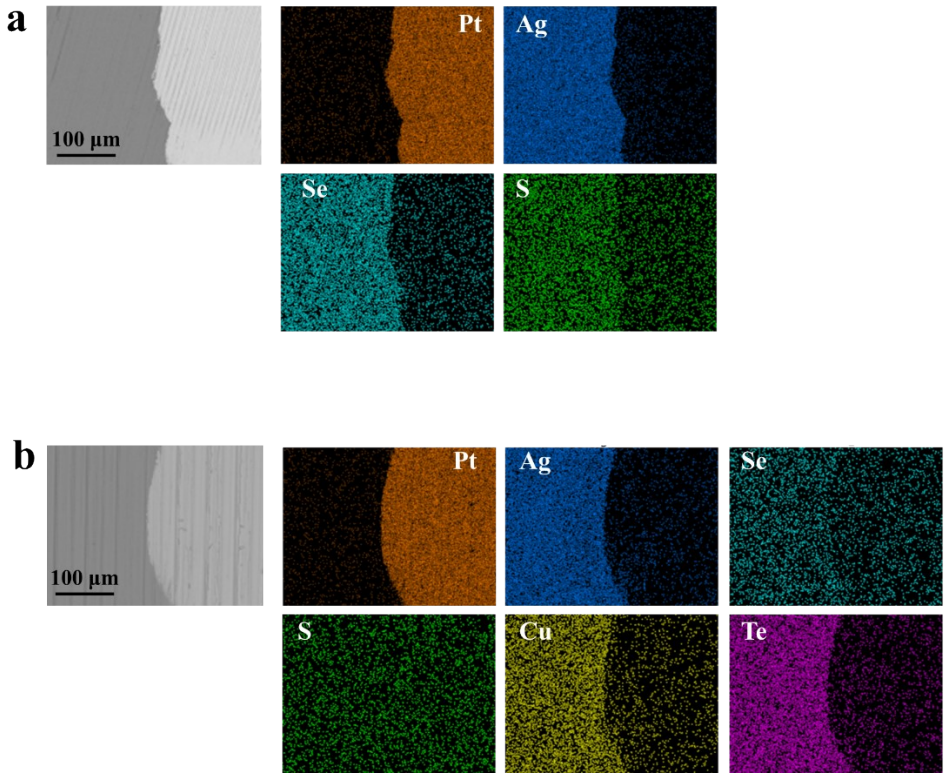

Fig. S6 Backscattered electron image and elemental energy dispersive spectroscopy (EDS) mappings at the (a) $Ag_2S_{0.33}Se_{0.67}$/Pt interface and (b) $Ag_{0.995}CuSe_{0.22}S_{0.08}Te_{0.7}$/Pt interface.

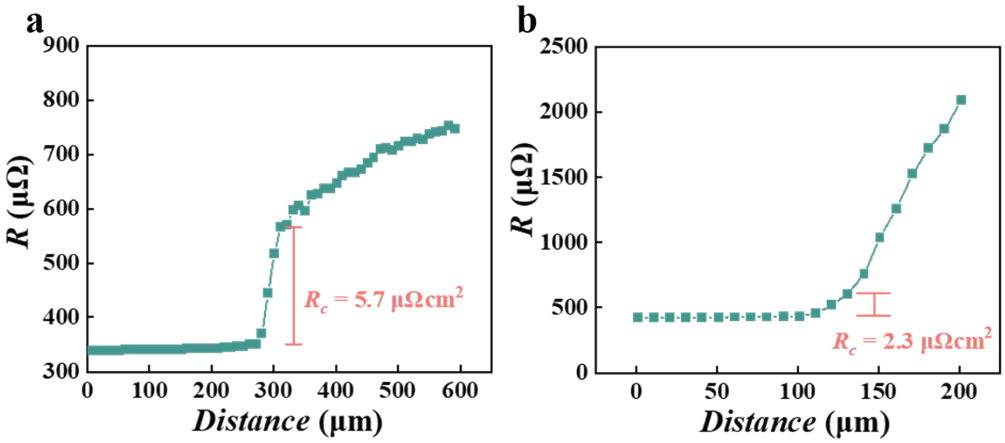

Fig. S7 Resistance (*R*) line scanning across the (a) $Ag_2S_{0.33}Se_{0.67}$/Pt and (b) $Ag_{0.995}CuSe_{0.22}S_{0.08}Te_{0.7}$/Pt interfaces.

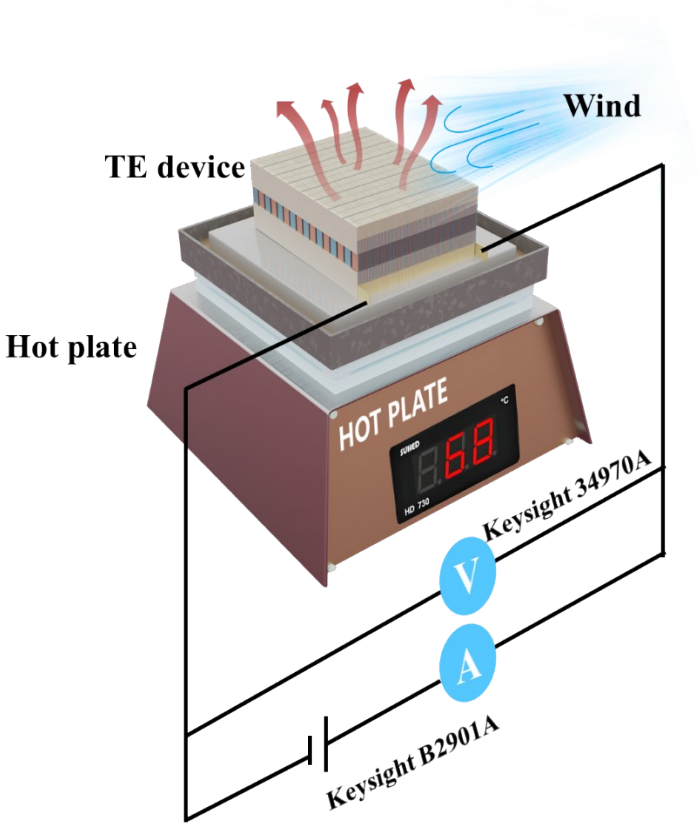

Fig. S8 Schematics of the homemade TE device test platform.

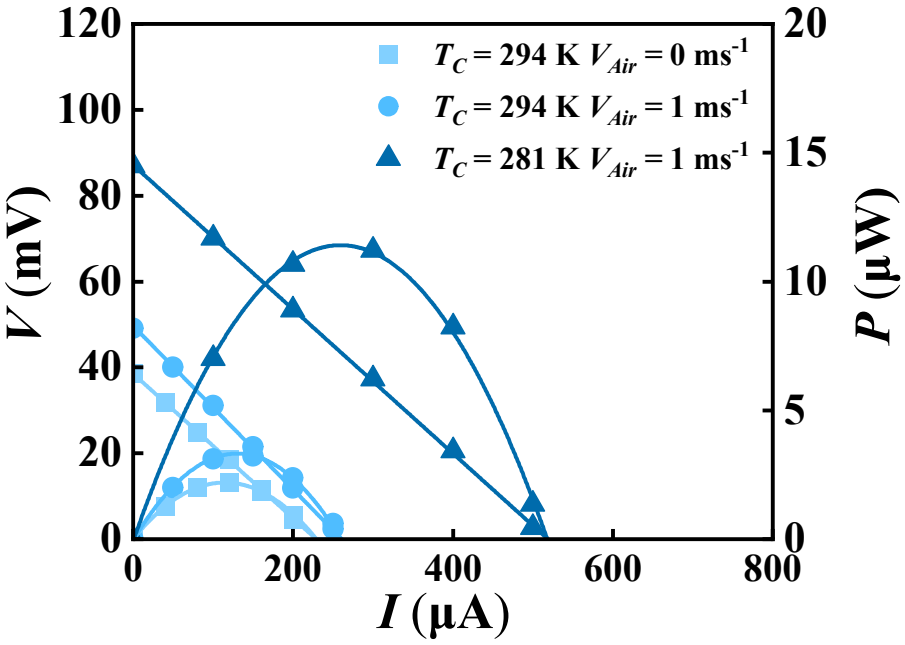

Fig. S9 Measured output power (P) and output voltage (V) as a function of current (I) for the 15-couple blade TE device under different cold-side temperatures (T_C) and different wind speeds (V_{Air}) when it is worn on human wrist.

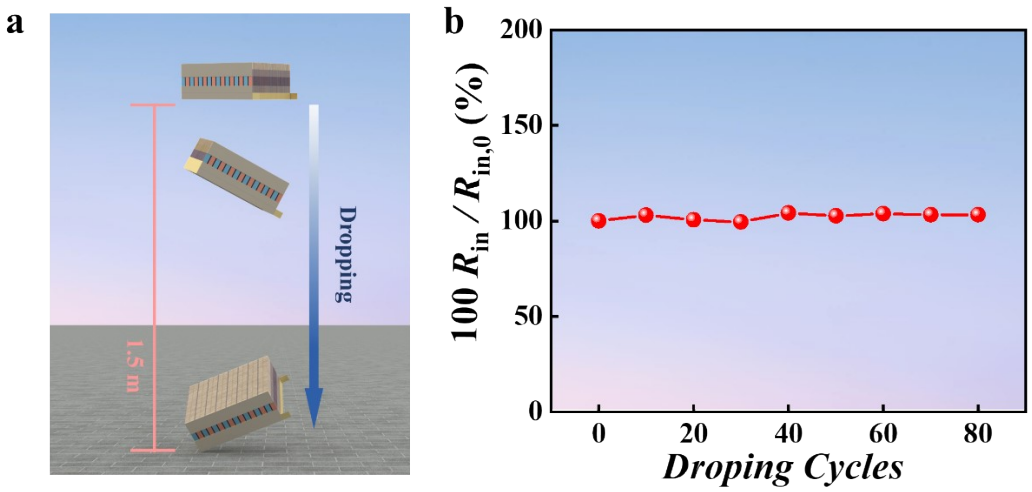

Fig. S10 (a) Schematic for the mechanical shock test. (b) Relative resistance changes of a blade TE device during the mechanical shock test.

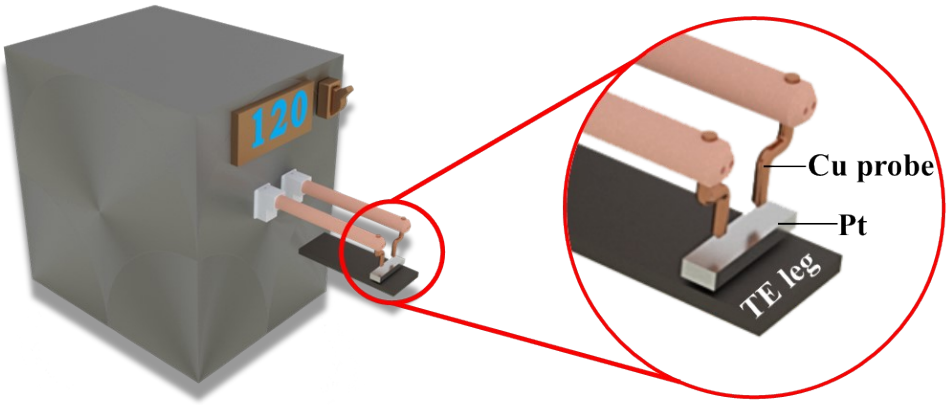

Fig. S11 Schematics of the spot-welding method used in this work.

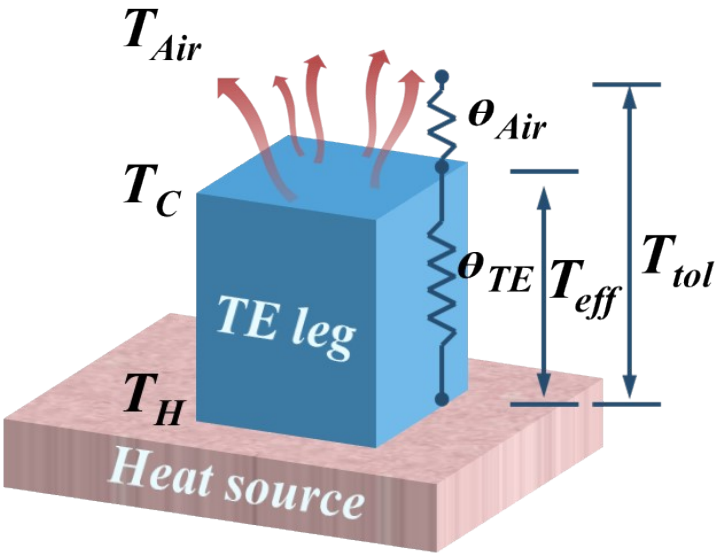

Fig. S12 Schematics for the simplified one-dimensional heat transfer model used for the derivation of maximum voltage density (V_{OC}/A) and power density (P_{max}/A).

Table S1 Comparison of the aspect ratio (H/S_{leg}) and density (n/A) of TE legs for typical TE devices. The maximum power density (P_{max}/A) and voltage density (V_{OC}/A)) of typical TE devices reported before. All data are collected in the wearing condition.

Type	*Shape*	H/S_{leg} (cm^{-1})	n/A (cm^{-2})	V_{oc}/A ($mVcm^{-2}$)	P_{max}/A (μWcm^{-2})	Ref.
Blade structure		1250	375	386.5 491.3 869.6	22 33.2 114.1	This work
Bulk	π-shaped	83	28	25.8	71.8	[1]
		87	42	33.4	43.6	[2]
		50	6	7	25.1	[3]
		15.6	2	2.5	18.4	[4]
		20	2	1.6	1.6	[5]
		30	34	33	42	[6]
		50	18	9.2	29	[7]
		4	4	1.8	20.6	[8]
		7.7	8	4.5	56	[9]
		8.2	8	7.75	138.46	[10]
		39	22	6.2	9.5	[11]
		8	4	3.3	73.7	[12]
Film	π-shaped	500	2	1.1	0.18	[13]
		2666.7	1	0.94	0.04	[14]
		25000	5	1.5	0.0043	[15]
		47619	3	1.4	0.00011	[16]
		1600	1	0.4	0.019	[17]
		3200	1	0.63	0.04	[18]
		5700	1	0.5	0.018	[19]
	Y-shaped	150	2	1.3	1.1	[20]
		321.4	3	2.28	2	[21]
	S-shaped	1040	3	0.33	0.0068	[22]

Table S2. Detailed materials' performance used for modeling the output performance of blade TE device in this work.

Materials	Seebeck coefficient (μVK^{-1})	Electrical conductivity (10^4 Sm^{-1})	Power factor ($\mu Wcm^{-1}K^{-2}$)	Thermal conductivity ($Wm^{-1}K^{-1}$)
$Ag_2S_{0.33}Se_{0.67}$	-130	10.6	17.9	1.1
$Ag_{0.995}CuSe_{0.22}S_{0.08}Te_{0.7}$	216	1.09	5.08	0.33

References

1. W. Fan, Z. An, F. Liu, Z. Gao, M. Zhang, C. Fu, T. Zhu, Q. Liu and X. Zhao, *Adv. Sci.*, 2023, **10**, 2206397.
2. W. Fan, Z. Shen, Q. Zhang, F. Liu, C. Fu, T. Zhu and X. Zhao, *ACS Appl. Mater. Interfaces*, 2022, 14, 21224-21231.
3. S. Hong, Y. Gu, J. K. Seo, J. Wang, P. Liu, Y. S. Meng, S. Xu and R. Chen, *Sci. Adv.*, 2019, **5**, eaaw0536.
4. L. Miao, S. Zhu, C. Liu, J. Gao, Z. Zhang, Y. Peng, J.-L. Chen, Y. Gao, J. Liang and T. Mori, *Nat. Commun.*, 2024, **15**, 8516.
5. B. Wu, Y. Lin, Y. Tian, W. Wei, Y. Xu, Y. Hu, J. Li, K. Li, C. Hou, Q. Zhang, Y. Li and H. Wang, *Adv. Funct. Mater.*, 2024, **34**, 2402319.
6. X. Yuan, P. Qiu, C. Sun, S. Yang, Y. Wu, Y. Wang, M. Gu, L. Chen and X. Shi, *Energy Environ. Sci.*, 2025, **18**, 5416-5423.
7. S. Zhu, Y. Peng, J. Gao, L. Miao, H. Lai, C. Liu, J. Zhang, Y. Zhang, S. Zhou, K. Koumoto and T. Zhu, *ACS Appl. Mater. Interfaces*, 2021, **14**, 1045-1055.
8. Y. Liu, L. Yin, W. Zhang, J. Wang, S. Hou, Z. Wu, Z. Zhang, C. Chen, X. Li, H. Ji, Q. Zhang, Z. Liu and F. Cao, *Cell Rep. Phys. Sci.*, 2021, **2**, 100412.
9. S. Bao, W. Zhu, Y. Yu, L. Liang and Y. Deng, *ACS Appl. Eng. Mater.*, 2023, **1**, 660-668.
10. X. Yuan, Z. Li, Y. Shao, D. Yang, K. Hu, H. You, Z. Xu, S. Hua, W. Liu, P. Peng, Y. Yan and X. Tang, *J. Mater. Chem. C*, 2022, **10**, 6456-6463.
11. K. Chen, Y. Yan, X. Sun, X. Li, D. Ma, Y. Li, S. Li, W. Zhang and Y. Deng, *Adv. Energy Mater.*, 2025, **n/a**, e03184.
12. Y. Jing, J. Luo, X. Han, J. Yang, Q. Liu, Y. Zheng, X. Chen, F. Huang, J. Chen, Q. Zhuang, Y. Shen, H. Chen, H. Zhao, G. J. Snyder, G. Li, T. Zhang and K. Zhang, *Energy Environ. Sci.*, 2023, **16**, 4334-4344.
13. Q. Zhou, K. Zhu, J. Li, Q. Li, B. Deng, P. Zhang, Q. Wang, C. Guo, W. Wang and W. Liu, *Adv. Sci.*, 2021, **8**, 2004947.
14. W. Chen, X.-L. Shi, M. Li, T. Liu, Y. Mao, Q. Liu, M. Dargusch, J. Zou, G. Q. Lu and Z.-G. Chen, *Science*, 2024, **386**, 1265-1271.
15. S. Hwang, D. Jang, B. Lee, Y. S. Ryu, J. Kwak, H. Kim and S. Chung, *Adv. Energy Mater.*, 2023, **13**, 2204171.
16. Q. Zou, H. Shang, D. Huang, B. Xie, L. Zhang, K. Wang, H. Dong, C. Li, H. Gu and F. Ding, *Appl. Phys. Lett.*, 2022, **120**, 023903.
17. W. Chen, M. Li, X. Wang, J. Otte, M. Zhang, C. Zhang, T. Cao, B. Hu, N. Li, W.-D. Liu, M. Dargusch, J. Zou, Q. Sun, Z.-G. Chen and X.-L. Shi, *Nat. Commun.*, 2025, **16**, 7579.
18. L. Zhang, X.-L. Shi, H. Shang, H. Gu, W. Chen, M. Li, D. Huang, H. Dong, X. Wang, F. Ding and Z.-G. Chen, *Nat. Commun.*, 2025, **16**, 5002.
19. Y. Liu, Y. Lu, Z. Wang, J. Li, P. Wei, W. Zhao, L. Chen and K. Cai, *J. Mater. Chem. A*, 2022, **10**, 25644-25651.
20. X. Yuan, P. Qiu, C. Sun, S. Yang, Y. Wu, L. Chen and X. Shi, *Energy Environ. Sci.*, 2024, **17**, 4968-4976.
21. T. Deng, Z. Gao, Z. Li, P. Qiu, Z. Li, X. Yuan, C. Ming, T.-R. Wei, L. Chen and X. Shi, *Science*, 2024, **386**, 1112-1117.

22. H. Lv, L. Liang, Y. Zhang, L. Deng, Z. Chen, Z. Liu, H. Wang and G. Chen, *Nano Energy*, 2021, **88**, 106260.